Swift heavy ion irradiation induced interactions in the UMo/X/Al trilayer system (X= Ti, Zr, Nb, and Mo)

H-Y. Chiang[1*], S.-H. Park[2], M. Mayer[3], K. Schmid[3], M. Balden[3], U. Bösenberg[4], R. Jungwirth[1#], G. Falkenberg[4], T. Zweifel[1], W. Petry[1]

[1]Heinz Maier-Leibnitz Zentrum (MLZ), Technische Universität München, Lichtenbergstr. 1, 85747 Garching, Germany

[2]Sektion Kristallographie, Ludwig-Maximilians-Universität München, Theresienstr.41, 80333, München, Germany

[3]Max-Planck-Institut für Plasmaphysik, Boltzmannstr.2, 85748 Garching, Germany

[4]Deutsches Elektronen-Synchrotron DESY, Notkestr. 85, 22607 Hamburg, Germany

*Corresponding author:

Tel: +49-89 289 12695

Email: hsin-yin.chiang@frm2.tum.de

[#]Now at European Commission, Joint Research Centre, Institute for Transuranium Elements, Via Enrico Fermi 2749, 21027 Ispra, Italy

Abstract

Uranium-molybdenum (UMo) alloy embedded in an Al matrix (UMo/Al) has been considered as a promising candidate for fuel conversion of research reactors. A modified system with a diffusion barrier, UMo/X/Al trilayer (X = Ti, Zr, Nb, and Mo), has been investigated in order to suppress interdiffusion between UMo and the Al matrix. The trilayer was tested by swift heavy ion irradiation, followed by Rutherford backscattering spectroscopy (RBS) and X-ray microdiffraction (μ-XRD). Atomic mixing at the interfaces was resolved by RBS, indicating that Ti interacts strongly with UMo while Zr does with Al. μ-XRD revealed the formation of intermetallic AlX compounds which can detain further atomic mixing. However, Ti and Zr as diffusion barrier can be controversial because their presence might lead to γ-UMo decomposition. This study presents the effectiveness of diffusion barriers and the irradiation-induced phase impacting on the properties of the UMo/X/Al trilayer.

Keywords: Intermetallics, Swift heavy ion irradiation, RBS, μ-XRD, Diffusion, U-Mo fuel

1. Introduction

In the pursuit of lower U-enriched fuel in research reactors, U-based fuel with high densities will be necessary to compensate for the loss in U-enrichment in the fuel elements. The U_xMo (x= 7 - 10 wt %) alloy, denoted as UMo, is a promising candidate as a high density fuel because i) fission gases can be well-accommodated inside UMo up to a high fission density [1]; ii) the desired cubic γ-UMo phase is stabilized during in-pile irradiation [2]; iii) this alloy allows a high U densities up to 8 g/cm^3 in UMo powder dispersed in an Al matrix (UMo/Al) [3] or up to 16 g/cm^3 in monolithic UMo foils [4].

Post-irradiation examination of in-pile irradiated fuel test plates revealed the growth of an interdiffusion layer (IDL) between UMo and Al [5, 6]. The accommodation of large fission gas bubbles along the outer mantle of the IDL leads to fuel swelling [7, 8] and a decrease of thermal conductivity [9, 10]. As a consequence, the irradiation performance of UMo/Al fuel is degenerated. In order to suppress undesired UMo-Al interactions it is necessary to modify the UMo/Al interface. One of the propositions is to introduce a diffusion barrier into the UMo/Al system. The ideal barrier material should satisfy the following conditions: i) atomic transport between UMo and Al across the barrier should be detained or even blocked; ii) the barrier should be thermodynamically stable against UMo and Al. If any intermetallic phase is formed, it should be stable under irradiation; iii) the barrier should have high thermal conductivity and high mechanical resistance; iv) the neutron absorption cross section of the barrier should be within an acceptable value to minimize the loss of neutron flux; v) the barrier material should be compatible with processing procedures for spent fuel. To meet the criteria, transition metals X such as Ti, Zr, Nb [11, 12] and Mo [13] have been suggested as the barrier materials.

In the present work swift heavy ion irradiation [14, 15, 16] has been applied to study the stability of the UMo/X/Al trilayer. The trilayer was irradiated with ^{127}I ions at 80 MeV to

simulate irradiation damage caused by fission fragments during in-reactor operation. The applied ion species and energy are the typical conditions of fission fragments. During irradiation, interactions at both the UMo/X and the X/Al interfaces are expected. However, the system of ion irradiation is in a non-equilibrium status, which makes it difficult to predict the irradiation-induced phases. To characterize atomic mixing and phases induced by swift heavy ion irradiation in this complex system, RBS and μ-XRD have been applied. The findings will support the discussion of the modified properties (strength, ductility, etc.) and the evaluation of the UMo/X/Al trilayer for advanced UMo/Al fuels.

2. Experimental methods

2.1 Preparation of UMo/X/Al trilayer samples

Each UMo/X/Al trilayer was prepared by DC-magnetron sputtering in an ultra-high vacuum system. The diffusion barrier, denoted as X, was produced by sputtering the metal ingot upon a polycrystalline Al substrate up to 0.5 - 4 μm in thickness. Subsequently, a depleted U8wt%Mo layer was sputtered upon the X/Al bilayer. Thicknesses of all layers are noted in Table 1. Swift heavy ion irradiation using ^{127}I ions at 80 MeV irradiated the UMo/X/Al trilayer perpendicularly to the UMo surface. The ion flux was set to 1.7×10^{12} ions /(s·cm^2) and the final ion fluence reached 10^{17} ions / cm^2 after about 17 hours. This ion fluence is equivalent to a low burnup value, i.e. below 10% of the peak burnup in the fuel elements of high performance research reactors such as FRM II [16]. The irradiation was carried out at 200°C which is the maximum temperature in the pin type fuel of research reactors during operation [17]. The experimental setup was adapted to ensure a stable irradiation temperature within a deviation of ± 2°C [18].

Monte Carlo calculations using the SRIM code stopping range of ions in matter (SRIM 2008) [19] predict the mean penetration depths of ^{127}I and the stopping powers, i.e. energy loss of

^{127}I ions, along the ion trajectory (Figure 1). These calculations indicate that the ^{127}I ions penetrate both interfaces of the trilayer, i.e. the UMo/X and the X/Al interfaces. The energy loss in the UMo/X/Al trilayer is dominated by electronic stopping power as shown in Figure 1B.

2.2 Focused ion beam milling (FIB) and scanning electron microscopy (SEM)

A thin foil of an UMo/X/Al trilayer cross-section was prepared by FIB [20] on a Zeiss Crossbeam NVision40. The thin foil was made by fine trenching from the swift heavy ion irradiated UMo/X/Al surface into the interfaces. The so-produced 2 μm thin foil with a section of 5 × 10 μm^2 was attached to a copper grid by carbon deposition. In addition, cross-sections of the UMo/X/Al trilayer were characterized by SEM using secondary electrons in the in-lens mode.

2.3 Rutherford backscattering spectrometry (RBS)

RBS measurements were performed at a 3 MV tandem accelerator of the Max-Planck Institut für Plasma Physik, Garching (Germany). Protons with 2.5 MeV penetrate perpendicularly on the UMo/X/Al trilayer with a beam size of 0.5 × 0.5 mm^2. The scattering angle θ was 165° and the final accumulated charge was 5 μC. The mean surface roughness R_a of the UMo/X/Al trilayer was observed by confocal microscopy and the value was within an acceptable value (i.e. R_a ~ 40 nm), i.e. considerably below the observed broadening of the interfaces. This enables further data analysis of elemental depth profiles.

2.4 μ-XRD with a synchrotron radiation

Synchrotron scanning X-ray microdiffraction measurements coupled with microscopic X-ray fluorescence mapping were performed at the microprobe experiment of the Hard X-ray

Micro/Nano-Probe beamline P06 at the storage ring PETRA III at the Deutsches Elektronen-Synchrotron (DESY) in Hamburg, Germany [21]. A primary energy of 21 keV was selected by means of a cryogenically cooled Si (111) double crystal monochromator. The beam was focused to 0.4 × 0.35 μm^2 (hor. × ver.) employing a Kirkpatrick-Baez mirror optic. The flux in the focused beam was ~10^{10} photons. A Keyence optical microscope was used for positioning of the thin foil UMo/X/Al cross-sections. XRD signals were recorded in transmission geometry with a 2k × 2k MAR sx165 CCD detector with 80 × 80 μm^2 effective pixel size and 165 mm scintillator screen diameter. X-ray fluorescence (XRF) signals were detected by means of a VORTEX EX Si-drift detector (SII Nano Technology) with 50 mm^2 active area and were applied to align the samples. Series of one-dimensional scans with 0.3 µm step size were carried out across the interfaces of the UMo/X/Al trilayer. An exposure time of 20 seconds per scan point was chosen in order to accommodate for the differences in atomic scattering factors, which is 9 times larger of U compared to that of Al [22].

3. Results

3.1 Characterization of cross-sections by SEM

Cross-sections of the irradiated UMo/X/Al trilayer have been characterized by SEM using secondary electrons in the in-lens mode. Due to the limited Z-contrast of SEM, the intermetallics formed in UMo/X/Al during swift heavy ion irradiation cannot be discriminated as shown in Figure 2A, -C, and -D. As an exception, a homogeneous layer with a thickness of 350 nm has been detected beneath the Zr layer (Figure 2B) in the UMo/Zr/Al trilayer, which has been identified as Al_3Zr by µ-XRD (see Section 3.3.4).

3.2 RBS data analysis: Concentration profiles

RBS spectra of the UMo/X/Al trilayer have been acquired at both the non-irradiated and the ^{127}I ion irradiated areas. As shown in Figure 3, the UMo layer locates at the high energy edge followed by the diffusion barrier and Al. Irradiation-induced atomic mixing can be recognized by the smearing of the high energy edge at the interfaces (i.e. the slope of the high energy edge decreases), or by the peak broadening of diffusion barrier material at lower energies after swift heavy ion irradiation. Note the intensity decrease in the high energy edge comes from the surface oxidation during the swift heavy ion irradiation.

Atomic mixing at the interfaces was calculated by SIMNRA software [23] quantitatively to obtain the elemental depth profiles, i.e. atomic concentration of elements versus areal density (atoms/cm^2). Figure 4 shows that at the irradiated area the interfaces exhibit atomic mixing prominently by the mixed elemental depth profiles. Especially at the X/Al interfaces atomic mixing took place aggressively, pointing out a strong interaction between the transition metals and Al. By comparing elemental depth profiles of the non-irradiated and of the irradiated areas, atomic mixing induced by swift heavy ion irradiation can be observed.

The intermixed region Δh at the interface of the UMo/X/Al trilayer can be calculated as

$$\Delta h = h^{irradiated} - h^{non-irradiated} = \left(\frac{D}{\rho_{mix}}\right)^{irradiated} - \left(\frac{D}{\rho_{mix}}\right)^{non-irradiated} \quad (1)$$

where h (cm) is the interfacial region, D (atoms/cm^2) is the areal density provided by SIMNRA, and ρ_{mix} is the local atomic density (atoms/cm^3). ρ_{mix} can be assumed as $\frac{1}{\rho_{mix}} = \sum_i \frac{C_i}{\rho_i}$, where C_i and ρ_i correspond to the concentration and to the bulk atomic density of element i [24], respectively. The prerequisites involve two assumptions: i) the elemental layers have the elemental bulk densities; ii) the volume per atom in the intermixed region is the same as in the pure element. The intermixed regions estimated for the UMo/X/Al trilayer (X = Ti, Zr, and Nb) are given in Table 2. The intermixed region in the UMo/Mo/Al trilayer cannot be estimated due to the extremely thin Mo layer (~ 300 nm), where the elemental

depth profile of U overlaps with that of Al in the Mo layer. Results from SIMNRA calculations showed that Ti interacts strongly with UMo in comparison to Zr and Nb. On the other hand, the intermixed region of Al with Zr is much larger than with Ti or with Nb. Among the transition metals, Nb is relatively inert to both UMo and Al. Atomic mixing of the UMo/X/Al trilayer as characterized by XRF gives qualitatively the similar result.

In addition to atomic mixing, the presence of irradiation-induced phases can be observed by those steps in the RBS spectra, which can be addressed to the existence of constant compositions. A step near the UMo/Ti interface, i.e. at the channel number ~ 390, was found in the UMo/Ti/Al trilayer. Also a step was found near the Mo/Al interface (at the channel number ~ 380), in the UMo/Mo/Al trilayer. The identification of the irradiation-induced steps and the broadening of flat-top peaks in RBS spectra have been quantitatively verified by μ-XRD, as shown in the following section.

3.3 X-ray diffraction data analysis

3.3.1 Rietveld refinement

The 2D μ-XRD patterns were corrected for dark field and converted into a 1D pattern using the software package Fit2D [25]. Phase identification was processed by the interface software Match! [26] based on the data bank Inorganic Crystal Structure Database (ICSD) [27]. Rietveld refinement analysis was applied using the software package Fullprof [28]. Deformation and recrystallization texture by swift heavy ion irradiation were taken into consideration in Rieveld refinement in combination of March-Dollase multiaxial preferred orientation after refining peak shapes using the Pseudo-Voigt profile function.

3.3.2 UMo/Ti/Al trilayer

Figure 5 presents typical μ-XRD patterns of the UMo/Ti/Al trilayer from the UMo region (Figure 5A), the UMo/Ti interface (Figure 5B), and the Ti/Al interface (Figure 5C); in the UMo region, γ-UMo (space group symmetry: **I**m-3m), and UO_2 (**F**m-3m) are present. The Cu pattern (**F**m-3m) comes from the copper grid (the sample holder). Further UMo (**I**m-3m) and an intermetallic solid solution $Ti_{0.04}U_{0.96}$ (**C**mcm) could be identified at the UMo/Ti interface. $Ti_{0.04}U_{0.96}$ originates from a martensitic transformation of γ-U. This transformation occurs in the presence of a super-saturated Ti inside U [29] once the irradiation terminated. The crystal structure of $Ti_{0.04}U_{0.96}$ is essentially the same as that of α-U with a slight difference in their lattice parameters. The orthorhombic α-U phase is undesired in UX fuel since it causes anisotropic deformation during the thermal cycling process [30], reducing the corrosion resistance and the irradiation stability. On the other hand, γ-UX alloys in cubic structure are stable against deformation caused by irradiation. Nevertheless, Ti additions up to 2% can effectively increase the strength, hardness and corrosion resistance of martensitic U (i.e. α-U) but decrease the ductility at the same time [31, 32, 33].

At the Ti/Al interface UMo (**I**m-3m) and the intermetallic solid solution $Al_{0.3}Ti_{1.7}$ (**P**6_3mmc) are present. The crystal structure of $Al_{0.3}Ti_{1.7}$ is isostructural to Ti. During irradiation, the process of forming this intermetallic solid solution could lead to an anisotropic deformation accompanying a lattice expansion of Al (**F**m-3m). However, because of the partially filled d sub-shell of Ti the interatomic bonding strength of $Al_{0.3}Ti_{1.7}$ is expected to be higher than that of pure Al. This may be advantageous to protect the interface from further atomic mixing induced by ion collisions.

According to the Hume-Rothery rule [34], both $Ti_{0.04}U_{0.96}$ and $Al_{0.3}Ti_{1.7}$ belong to substitutional alloys. Upon the irradiation process solute Ti atoms of $Ti_{0.04}U_{0.96}$ and Al of $Al_{0.3}Ti_{1.7}$ were transported to the respective solvents α-U and Ti by replacing the native atoms

to form the solid solutions. Refined atomic parameters and concentrations of the phases found in the irradiated UMo/Ti/Al trilayer are listed in Table 3.

3.3.3 UMo/Zr/Al trilayer

μ-XRD patterns of the UMo/Zr/Al trilayer obtained at the UMo region (Figure 6A) show UMo (**I**m-3m) and UO_2 (**F**m-3m); near the UMo/Zr interface (Figure 6B) UMo (**I**m-3m) and Mo (**I**m-3m) are observed. The Mo phase comes from Mo segregation out of UMo alloy. This segregation can be explained from the viewpoint of thermodynamics: the high positive enthalpy of mixing ΔH_m between Zr and Mo (36 kJ/mol) prevents Mo atoms inside UMo alloy from mixing with Zr. As a consequence, the Mo phase forms. This Mo segregation causes a decrease of the local Mo concentration inside UMo alloy and then could decrease the γ-UMo stability [35, 36, 37]. However, there is no sign of γ-UMo decomposition into α-U, or any further destructive features at the UMo/Zr interface. Similarly, Mo-rich precipitates can occur during the hot-rolling process of the UMo/Zr/Al monolithic fuel, as reported [38].

At the Zr/Al interface, Zr (**P**6_3mmc), UMo (**I**m-3m), and the irradiation-induced compound Al_3Zr (**P**m-3m) could be identified. The intermetallic compound Al_3Zr typically crystallizes in the tetragonal **I**4/mmm structure, whereas the metastable cubic Al_3Zr (**P**m-3m) can be formed by rapid solidification or grown from a supersaturated solid solution [39, 40]. Cubic intermetallics are preferred phases due to their high ductility. In addition, Al_3Zr is densely packed with much stronger interatomic bonds compared to Zr. Such an intermetallic compound can prevent further atomic mixing between Zr and Al during the irradiation process. However, according to the broad Bragg's peaks, the crystallinity of Al_3Zr in the UMo/Zr/Al might be poor, e.g. nanocrystalline, which will affect its mechanical properties. Details of phase information of the UMo/Zr/Al trilayer are summarized in Table 4.

3.3.4 UMo/Nb/Al trilayer

Rietveld analysis with μ-XRD data of the three different regions, i.e. the UMo, the UMo/Nb interface, and the Nb/Al interface in the UMo/Nb/Al trilayer are graphically demonstrated in Figure 7. UMo (**I**m-3m) and UO_2 (**F**m-3m) are present in the UMo region (Figure 7A); UMo (**I**m-3m) and Nb (**I**m-3m) at the UMo/Nb interface (Figure 7B).

The Nb/Al interface (Figure 7C) contains UMo (**I**m-3m), Nb (**I**m-3m), $Mo_{0.1}Nb_{0.45}U_{0.45}$ (**I**m-3m), and Nb_3Al (**P**m-3n) in a poor crystalline state. The ternary alloy $Mo_{0.1}Nb_{0.45}U_{0.45}$ forms usually by heat treatments at 1350°C, such as alloying processes [41]. It has better irradiation resistance and corrosion resistance than the corresponding binary UX-alloys that can improve the U-based fuel properties [42, 43]. It is also known that an Nb addition of 1- 4% in the U-Mo-Nb system allows to retard transformations in γ-UMo alloys [44, 45]. Nb_3Al (**P**m-3n) can be produced at extremely high temperatures ($T \geq 2060°C$) [46] or under He ion irradiation [47]. Nb_3Al has been used for high temperature applications because of its high stability and strength. Therefore, this phase can serve as a barrier against the Nb-Al intermixing during irradiation. However, note the poor crystallinity of Nb_3Al in the UMo/Nb/Al trilayer could degenerate its stability and strength. Refined structural parameters and concentrations of all phases found in the UMo/Nb/Al trilayer are summarized in Table 5.

3.3.5 UMo/Mo/Al trilayer

μ-XRD patterns of the phases within the irradiated UMo/Mo/Al trilayer sample are shown in Figure 8. In the UMo region (Figure 8A) UMo (**I**m-3m) and UO_2 (**F**m-3m) are present; UMo (**I**m-3m) and Mo (**I**m-3m) coexist near the UMo/Mo interface (Figure 8B); UMo (**I**m-3m), Mo (**I**m-3m) and an irradiation induced compound $Al_{12}Mo$ (**I**m-3) are seen at the Mo/Al interface (Figure 8C).

$Al_{12}Mo$ can be formed in thermal processes at 400°C ≤ T ≤ 661°C, when the critical Mo content is lower than 10 at% [48]. Studies demonstrate this alloy possesses high strength due to the covalent directional bonding to configure densely packed layers [49, 50]. Hence, it is expected that the presence of $Al_{12}Mo$ can be advantageous at the Mo/Al interface to prevent further atomic mixing at the interface. Refined structural parameters and concentrations of all phases found in the UMo/Mo/Al trilayer are given in Table 6.

4. Discussion

4.1 Ion beam mixing: the ballistic effects

Ion beam mixing due to ballistic effects has been simulated for the UMo/X/Al trilayers (X = Ti, Zr, Nb, and Mo) by means of TRIDYN code [51]. TRIDYN simulates dynamic changes of thickness and composition of multicomponent targets during high-dose ion irradiation and allows to calculate the depth profiles of different atomic species in the target as function of the incident fluence. For those trilayers with a thick UMo layer (i.e. X = Ti, Zr, and Nb), the elemental depth profiles of the diffusion barriers are almost unchanged after irradiation. TRIDYN calculations show that ballistic effects only contribute to an intermixed region of ~ 10 nm in these trilayers, which is is beyond the resolution of RBS and relatively small compared to the RBS observations.

For the UMo/Mo/Al trilayer, with a relatively thin UMo layer, ion beam mixing by ballistic effects is more prominent - see Figure 9A. A comparison between the simulated and the initial Mo depth profiles points out that atomic mixing induced by ballistic effects is around 100 nm in the UMo/Mo/Al trilayer. In addition, a comparison of the UMo/Mo/Al trilayer between the TRIDYN calculations and the RBS spectrum is illustrated in Figure 9B. The deviation of Mo peak (~ channel number 600) of the TRIDYN calculations from the experimental result comes from the surface oxidation, which was not considered in TRIDYN

calculations. The width of Mo peak remains after swift heavy ion irradiation, indicating atomic mixing is below depth resolution of RBS. Furthermore, the tail of the RBS spectrum extended to low energies suggests the existence of another diffusion phenomenon. The discrepancy of TRIDYN calculations and the RBS spectrum indicates that ion beam mixing by ballistic effects is relatively small and can be practically neglected for the investigated ion fluences.

4.2 Thermodynamic effects in ion mixing

Considering the UMo/Zr/Al and the UMo/Nb/Al trilayers, both should exhibit the same ballistic response to ion mixing because their nearly identical parameters for ion-solid interactions, i.e. atomic density, atomic number, and atomic mass. However, RBS data analysis indicates that the UMo/Zr/Al trilayer interfaces are well-intermixed, whereas the interfaces in the UMo/Nb/Al trilayer are relatively unaltered after irradiation. This disparity might result from the difference in ΔH_m of the two trilayers. Calculations applying Miedema's model [52, 53] for the ΔH_m of the U-X and the X-Al binary solid solutions are illustrated in Figure 10. Figure 10A demonstrates that Ti has a tendency to form a U-Ti alloy, whereas other transition metals are relatively inert. Nb has a larger $+\Delta H_m$ against forming the U-Nb alloy in comparison to Zr. In Figure 10B one can recognize that the applied transition metals are all in favor of forming X-Al solid solutions. In particular, Zr has a high tendency to the formation of Zr-Al solid solutions in comparison to Ti, Nb, and Mo. This prediction using ΔH_m is well in accord with observations in RBS. In combination of the result from TRIDYN simulations and the good agreement of ΔH_m prediction, one can assume that chemical potentials play an important role in atomic mixing during swift heavy ion irradiation and dominate over ballistic effects.

4.3 RBS v.s. μ-XRD

The steps observed in the RBS spectra of the UMo/Ti/Al and the UMo/Zr/Al trilayers can be explained by the presence of $Ti_{0.04}U_{0.96}$ and $Al_{12}Mo$, respectively, based on their typical reflections detected in spatially-resolved μ-XRD pattern. Some of the intermetallic compounds identified in μ-XRD can be seen in the elemental depth profiles of RBS, as well. Nb_3Al in the UMo/Nb/Al trilayer were observed in the depth profile at the Nb/Al interface, giving the atomic ratio of Nb: Al = 7: 3 (see Figure 4C near the depth 25000 × 10^{15} atoms/cm^2). $Al_{12}Mo$ in the UMo/Mo/Al trilayer shows an atomic ratio of Al: Mo = 9: 1 (see Figure 4D in the depth 13000 × 10^{15} atoms/cm^2). The atomic ratio evaluated from RBS differs from that from μ-XRD. This discrepancy can be explained by the limited resolution of RBS in probing the UMo/X/Al trilayer system: the UMo layer has a high density (17.7 g/cm^3) and this layer is relatively thick compared to usual RBS studies dealing with around 100 nm thin layers.

The combination of RBS and μ-XRD allows an overall understanding of the UMo/X/Al trilayer after irradiation. From the RBS measurements we have obtained the information about atomic mixing via elemental depth profiles, which is non-trivial to obtain from μ-XRD mainly due to extremely different atomic scattering factors in UMo/X/Al systems. On the other hands, qualitative and quantitative phase analysis could be performed with spatially resolved μ-XRD data. By applying this combination of methods it was possible to characterize several intermetallic compounds in the UMo/X/Al tirlayer.

5. Summary

The current study shows that the application of a diffusion barrier using transition metals in UMo/X/Al allows suppressing the UMo-Al interactions completely. Besides, atomic mixing at interfaces, such as UMo-X and X-Al intermixing, was limited maximal up to ~ 0.5 μm. Ti,

Zr, Nb and Mo form intermetallics with Al, and these irradiation-induced compounds can act as additional interdiffusion barriers at the X/Al interface. However, Ti and Zr as the diffusion barriers might lead to γ-UMo decomposition by forming the orthorhombic U-Ti compound and segregating Mo from UMo, respectively. Nb as the diffusion barrier behaves stable at both the UMo/Nb and the Nb/Al interfaces while the poor crystallinity of the Nb-Al compound can be a concern. In conclusion Mo is the most promising candidate for diffusion barriers in UMo/X/Al systems with its high strength Mo-Al compound to protect the interface from further ion collisions.

Acknowlegdement

We acknowledge DESY for providing beamtime via project, I-20120422. S. Klaumünzer at HZB and H. Palancher at CEA are acknowledged for scientific discussions. This work was supported financially by the German federal ministry for science and technology (BMBF) and the Bavarian ministry for education and science (StMBW) (project FRM0911). Part of this project has received funding from the Euratom research and training programme 2014-2018.

Reference

[1] G.L. Hofman et al., *Recent observations at post-irradiation examination of low-enriched UMo miniplates irradiated to high burnup* in proceedings of the 25th International Topical Meeting on Reduced Enrichment for Research and Test Reactors (RERTR), Chicago, 2003

[2] M.L. Bleiberg L.J. Jones, B. Lustman, Journal of Applied Physics, 27 (1956) 1270

[3] M.A. Leeser et al., *Radiation stability of fuel elements for the Enrico Fermi power reactor* in proceedings of the second international conference on the peaceful uses of atomic energy/5, page 587, New York, 1958

[4] R.M. Hengstler, L. Beck, H. Breitkreutz, C. Jarousse, R. Jungwirth, W. Petry, W. Schmid, J. Schneider, N. Wieschalla, J. Nucl. Mater. 402 (2006) 74

[5] J.L. Snelgrove et al., *Development of very-high-density fuels by RERTR program* in proceedings of the 19th International Topical Meeting on Reduced Enrichment for Research and Test Reactors (RERTR), Seoul, 1996

[6] M.K. Meyer et al., *Metallographic analysis of irradiated RERTR-3 fuel test specimens* in proceedings of 23rd International Meeting on Reduced Enrichment for Research and Test Reactors (RERTR), Las Vegas, 2000

[7] J.M. Hamy et al., *The French UMo group contribution to new LEU fuel development* in proceedings of 9th International Topical Meeting on Research Reactor Fuel Management (RRFM), Budapest, 2005

[8] J.M. Park et al., *Phase stability and diffusion characteristics of U-Mo-X (X=Si, Al, Zr or Ti) alloys* in proceedings of the 27th International Topical Meeting on Reduced Enrichment for Research and Test Reactors (RERTR), Boston, 2005

[9] S.H. Lee, J.C. Kim, J.M. Park, C.K. Kim, S.W. Kim, Int. J. Thermophys., 2003, 24(5) 1355

[10] J. Gan, D.D. Keiser Jr., B.D. Miller, A.B. Robinson, J.F. Jue, P. Medvedev, D.M. Wachs, J. Nucl. Mater. 424 (2012) 43

[11] G.A. Birzhevoy et al., *Results of post-irradiation examination of the (U-Mo) - Aluminum matrix interaction rate* in proceedings of the 11th International Topical Meeting on Research Reactor Fuel Management (RRFM), Lyons, 2007

[12] D.D. Keiser et al., *Characterization and testing of monolithic RERTR fuel plates* in proceedings of the 11th International Topical Meeting on Research Reactor Fuel Management (RRFM), Lyons, 2007

[13] K. Huang, Y. Park, D.D. Keiser, Y.H. Sohn, Journal of Phase Equilibria and Diffusion Vol. 34, 4 (2013) 307

[14]] N. Wieschalla, A. Bergmaier, P. Böni, K. Böning, G. Dollinger, R. Großmann, W. Petry, A. Röhrmoser, J. Schneider, J. Nucl. Mater. 357 (2006) 191

[15] H. Palancher, N. Wieschalla, P. Martin, R. Tucoulou, S. Sabathier, W. Petry, J-F. Berar, C. Valot, S. Dubois, J. Nucl. Mater. 385 (2009) 449

[16] R. Jungwirth, T. Zweifel, H-Y. Chiang, W. Petry, S. Van den Berghe, A. Leenaers, J. Nucl. Mater. 434 (2013) 296

[17] K.N. Choo, M.S. Cho, C.Y. Lee, S.W. Yang, S.J. Park, *Contribution of HANARO irradiation facilities to national nuclear R&D* in proceedings of International Symposium on Material Testing Reactor (ISMTR), Columbia, 2012

[18] H-Y. Chiang, T. Zweifel, H. Palancher, A. Bonnin, L. Beck, P. Weiser, M. Döblinger, C. Sabathier, R. Jungwirth, W. Petry, J. Nucl. Mater. 440 (2013) 117

[19] J.F. Ziegler, www.srim.org (2011)

[20] B.D. Miller, J. Gan, J. Madden, J.F. Jue, A. Robinson, D.D. Keiser, J. Nucl. Mater. 424 (2012) 38

[21] C.G. Shroer, P. Boye, J.M. Feldkamp, J. Patommel, D. Samberg, A. Schropp, A. Schwab, S. Stephan, G. Falkenberg, G. Wellenreuther, N. Reimers, Nucl. Instr. Meth. A 616 (2010) 93

[22] H.S. Peiser, H.P. Rooksby, A.J.C. Wilson, X-ray Diffraction by Polycrystalline Materials, The Institute of Physics, London (1955)

[23] M. Mayer, SIMNRA home page, www.simnra.com

[24] F.W. Walter, J.R. Parrington, F. Feiner, Nuclides and Isotopes (1989), General Electric Company

[25] H. Hammersley, www.esrf.eu/computing/scientific/FIT2D

[26] www.crystalimpact.com/match/

[27] www.fiz-karlsruhe.de/icsd

[28] J. Rodriguez-Carvajal, www.ill.eu/sites/fullprof, 2001

[29] A.M. Ammons, Physical Metallurgy of Uranium Alloys, edited by J.J. Burke, D.A. Colling, D.A.Gorum, J. Greenspan, pp. 511-585. Chestnut Hill, MA: Brook Hill

[30] N. E. Golovkina and V.K. Grigorovich, *Behavior of roller and normalized α-U alloys under conditions of thermal cycling* in Physical Chemistry of Alloys and Refractory Compounds of Thorium and Uranium edited by O.S. Ivanov, Keter Press (1972) 24

[31] Linard, M., *Study of Uranium-Titanium Alloys with a Low Titanium Content (0-1.5 Percent) by Weight*, translated from the French for Oak Ridge National Laboratory U.S. Atomic Energy Commission Contract Report No. ORNL-TR-2S79, Tennessee, 1971

[32] D.J. Murphy, Trans. ASM, 50 (1958) 884

[33] D.L. Douglass, Trans. ASM, 53 (1961) 307

[34] W. Hume-Rothery, R.E. Smallman, C.W. Haworth, The Structure of Metals and Alloys, The Institute of Metals, London, 1969

[35] J.M. Park et al., *Phase stability and diffusion characteristics of U-Mo-X (X=Si, Al, Zr or Ti) alloys* in proceedings of the 27th International Topical Meeting on Reduced Enrichment for Research and Test Reactors (RERTR), Boston, 2005.

[36] S. Dubois et al., *Development of dispersed UMo fuel: An oxide layer as a protective barrier of the UMo particles* in proceedings of the 28th International Meeting on Reduced Enrichment for Research and Test Reactors (RERTR), Cape Town, 2006

[37] G. Cabane, J. Nucl. Mater, 4 (1959) 364

[38] J.F. Jue, D.D. Keiser, C.R. Breckenridge, G.A. Moore, M.K. Meyer, J. Nucl. Mater. 448 (2014) 250

[39] E. Nes, Acta Metall. 20 (1972) 499

[40] T. Ohashi, R. Ichikawa, Metall. Trans. 3A (1972) 2300

[41] G.H. Bannister, J.R. Murry, J. of Less-Common metals, 2 (1960) 372

[42] L. Castaldelli, C. Fizzotti, A.G. Gandini, *Transformation Processes in Some Uranium Alloys Low in Molybdenum and Niobium* translated from the Italian for Sandia laboratories, U. S. Atomic Energy Commission Contract Report No. SC-T-72-2457, Albuquerque, 1972

[43] V.B. Kishinevskii, L. I. Gomozov, O.S. Ivanov, *Corrosion Resistance in Water of Some Alloys of Uranium with Zirconium, Niobium and Molybdenum* translated from Russian for University of California, U.S. Atomic Energy Commission Contract Report No. UCRL-Trans-10455, Lawrence Radiation Laboratory, Livermore, 1970

[44] R.J. van Thyne, D.J. McPherson, Amer. Soc. Metals Transactions 50 (1957) 576

[45] W.M. Justusson, J. Nucl. Mater. 4 (1961) 37

[46] J.L. Jorda, R. Flükiger, J. Muller, J. Less-Common Metals, 75 (1980) 227

[47] N. Li, M.S. Martin, O. Anderoglu, A. Misra, L. Shao, H. Wang, X. Zhang, J. App. Phy. 105 (2009) 123522

[48] L.K. Walford, Philos Mag., 9 (1964) 513

[49] G.T. Laissardiere, D.N. Manhm, D. Mayou, Prog. Mater. Sci. 50 (2005) 679

[50] H. Niu, X-Q. Chen, P. Liu, W. Xing, X. Cheng, D. Li, Y. Li, Scienitific report, 2 (2012) 718

[51] W. Möller, W. Eckstein, J. Nucl. Instr. Meth. B2 (1984) 814

[52] A.R. Meidema, A.K. Niessen, F.R. Boer, R. Boom, W.C.M Mattens, Cohesion in Metal: Transition Metal Alloys, Amsterdam, 1989

[53] R.F. Zhang, B.X. Liu, Applied Physics Letter, 81 (2002) 1219

Tables:

X / thickness	Ti	Zr	Nb	Mo
UMo layer (μm)	3.5	4.0	4.0	1.3
X layer (μm)	2.1	0.9	1.1	0.3

Table 1: Thicknesses of U/X/Mo layers for the samples investigated in this study.

$\Delta h_{UMo/X}$ (H^+)	X	$\Delta h_{X/Al}$ (H^+)
246 nm	Ti	360 nm
87 nm	Zr	534 nm
53 nm	Nb	110 nm

Table 2: Thicknesses of intermixed regions induced by swift heavy ion irradiation, as derived from RBS.

region	**(A) UMo**		**(B) UMo/Ti interface**		**(C) Ti/Al interface**	
phase	γ-UMo	UO_2	γ-UMo	$Ti_{0.04}U_{0.96}$	γ-UMo	$Al_{0.3}Ti_{1.7}$
concentration	81%	19%	82%	18%	75%	25%
space group	**I**m-3m	**F**m-3m	**I**m-3m	**C**mcm	**I**m-3m	**P**6_3mmc
lattice parameter (Å)	3.4068 (3)	5.433 (3)	3.4065(1)	a = 2.848(2) b = 5.831(2) c = 4.952(3)	3.4094(9)	a = 2.9686(3) c = 4.7852(9)

Table 3: Crystallographic information and concentrations of all phases identified within the irradiated UMo/Ti/Al trilayer sample.

region	**(A) UMo**		**(B) UMo/Zr interface**		**(C) Zr/Al interface**		
phase	γ-UMo	UO_2	γ-UMo	Mo	γ-UMo	Zr	Al_3Zr
concentration	92%	8%	80%	20%	4%	38%	58%
space group	**I**m-3m	**F**m-3m	**I**m-3m	**I**m-3m	**I**m-3m	**P**6_3mmc	**P**m-3m
lattice parameter (Å)	3.4080 (1)	5.450(1)	3.4077(4)	3.132(2)	3.4079 (4)	a = 3.2594(4) c = 5.03(1)	4.1297(7)

Table 4: Crystallographic information and concentrations of all phases identified within the irradiated UMo/Zr/Al trilayer sample.

region	**(A) UMo**		**(B) UMo/Nb interface**		**(C) Nb/Al interface**			
phase	γ-UMo	UO_2	γ-UMo	Nb	γ-UMo	Nb	$Mo_{0.1}Nb_{0.45}U_{0.45}$	Nb_3Al
concentration	99%	1%	26%	74%	6%	82%	11%	1%
space group	**I**m-3m	**F**m-3m	**I**m-3m	**I**m-3m	**I**m-3m	**I**m-3m	**I**m-3m	**P**m-3n
lattice parameter (Å)	3.3965 (1)	5.42 (3)	3.4134 (1)	3.3244 (4)	3.4184 (1)	3.3191 (7)	5.113(1)	3.3264 (2)

Table 5: Crystallographic information and concentrations of all phases identified within the irradiated UMo/Nb/Al trilayer sample.

region	**(A) UMo**		**(B) UMo/Mo interface**		**(C) Mo/Al interface**		
phase	γ-UMo	UO_2	γ-UMo	Mo	γ-UMo	Mo	$Al_{12}Mo$
concentration	89%	11%	94%	6%	44%	33%	23%
space group	**I**m-3m	**F**m-3m	**I**m-3m	**I**m-3m	**I**m-3m	**I**m-3m	**I**m-3
lattice parameter (Å)	3.4131 (1)	5.450(2)	3.3998(2)	3.1398(1)	3.4035(5)	3.150(2)	7.601(3)

Table 6: Crystallographic information and concentrations of all phases identified within the irradiated UMo/Mo/Al trilayer sample.

Figures and captions:

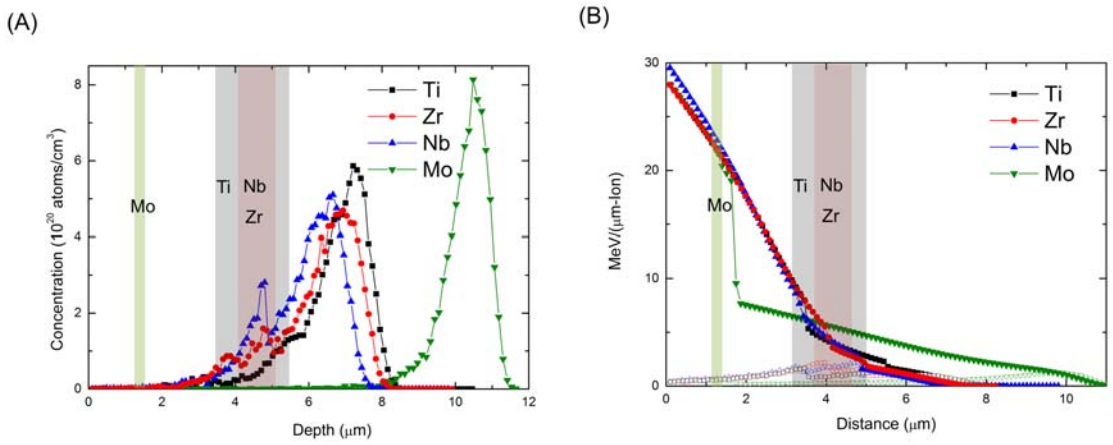

Figure 1: Comparison of penetration depth of ^{127}I (A) in and depth profiles of stopping powers (B) along the UMo/X/Al trilayers, have been obtained from SRIM calculations. Each barrier layer has been marked with the layer thicknesses given in Table 1. The range of ^{127}I indicates that the ions pass both the UMo/X and the X/Al interface. In the depth profiles of stopping powers, the electronic stopping (solid lines) dominates over the nuclear stopping (hollow lines) over most of the target range. The nuclear stopping becomes dominant only at the end of the ion range.

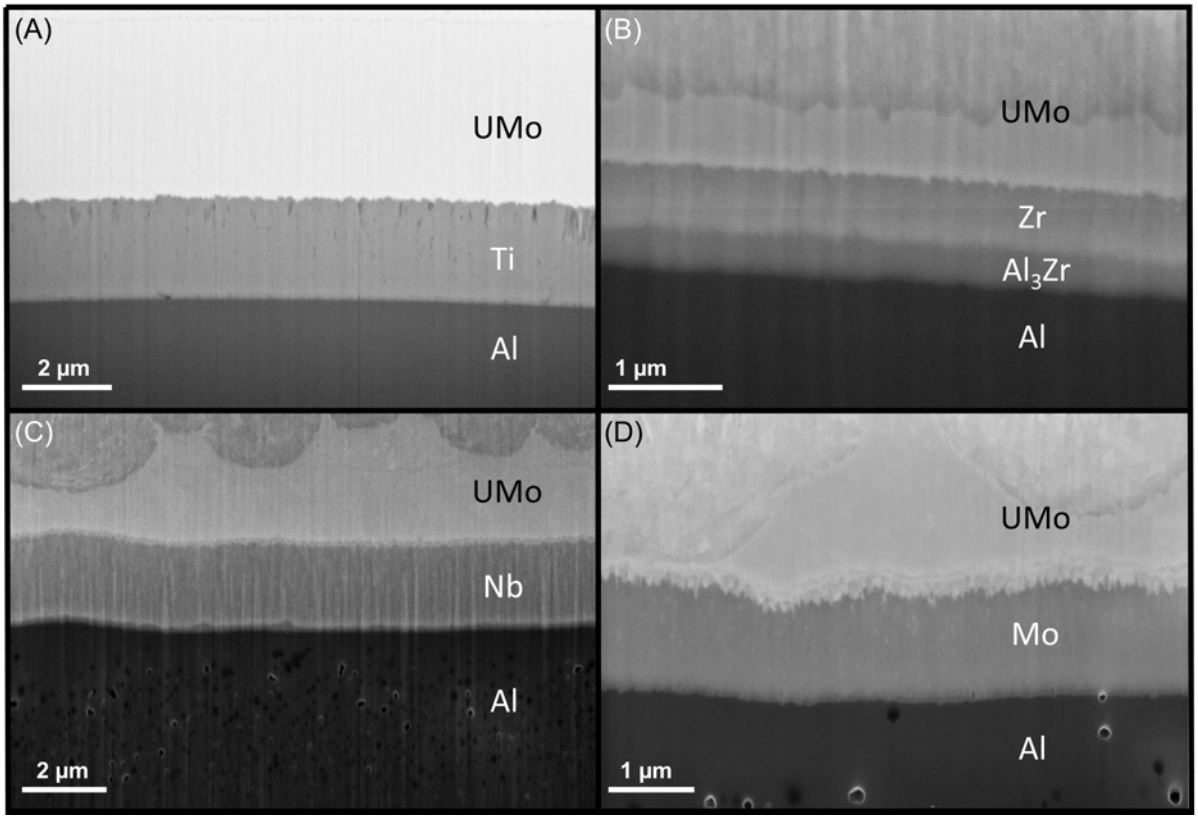

Figure 2: Cross sections of (A) the UMo/Ti/Al, (B) the UMo/Zr/Al, (C) the UMo/Nb/Al and (D) the UMo/Mo/Al trilayers prepared by FIB were characterized by SEM using secondary electrons in in-lens mode. Most intermetallic compounds induced by ion irradiaition could not be detected due to the limited Z-contrast of SEM. However, a homogeneous layer of the intermetallic compound Al_3Zr (~ 350 nm) formed beneath the Zr layer of the UMo/Zr/Al trilayer sample is well recognized by SEM (B).

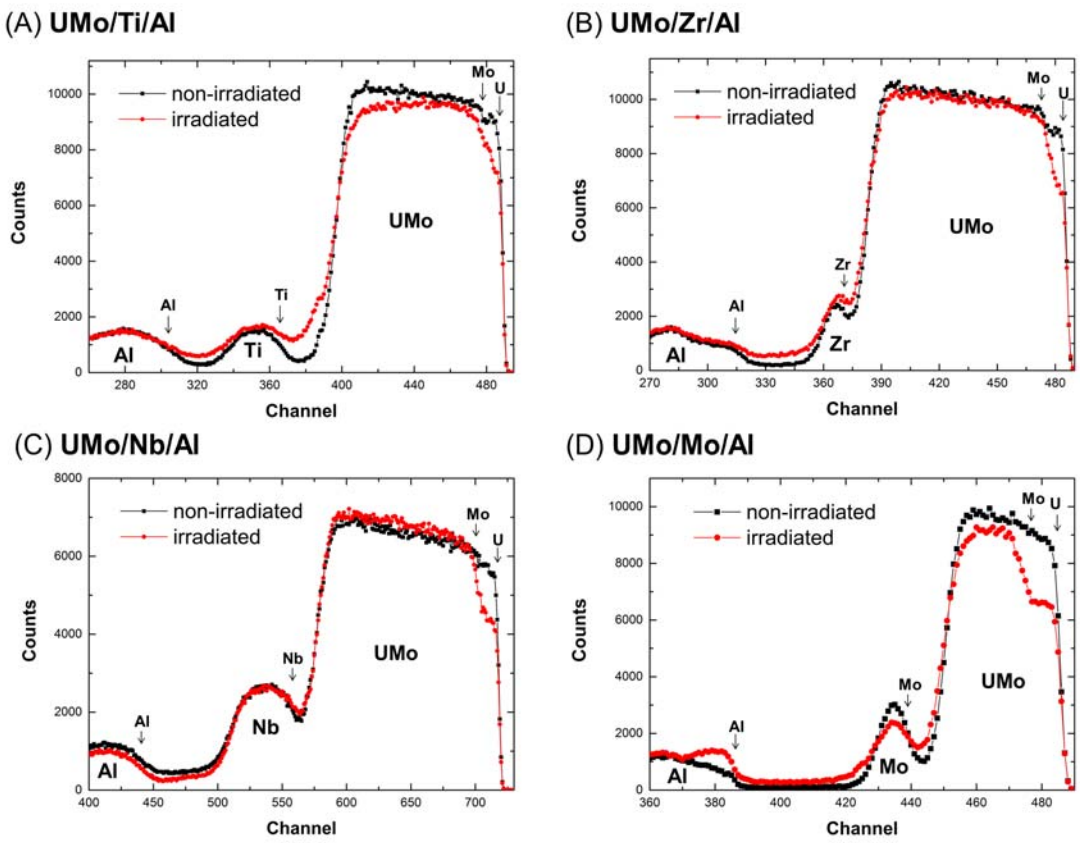

Figure 3: RBS spectra from both non-irradiated and irradiated areas of each UMo/X/Al trilayer (X = Ti (A), Zr (B), Nb (C), and Mo (D) where the backscattered ion energies of respective elements are marked. The atomic mixing at each UMo/X and X/Al interfaces are recognized by smeared or broadened RBS peaks.

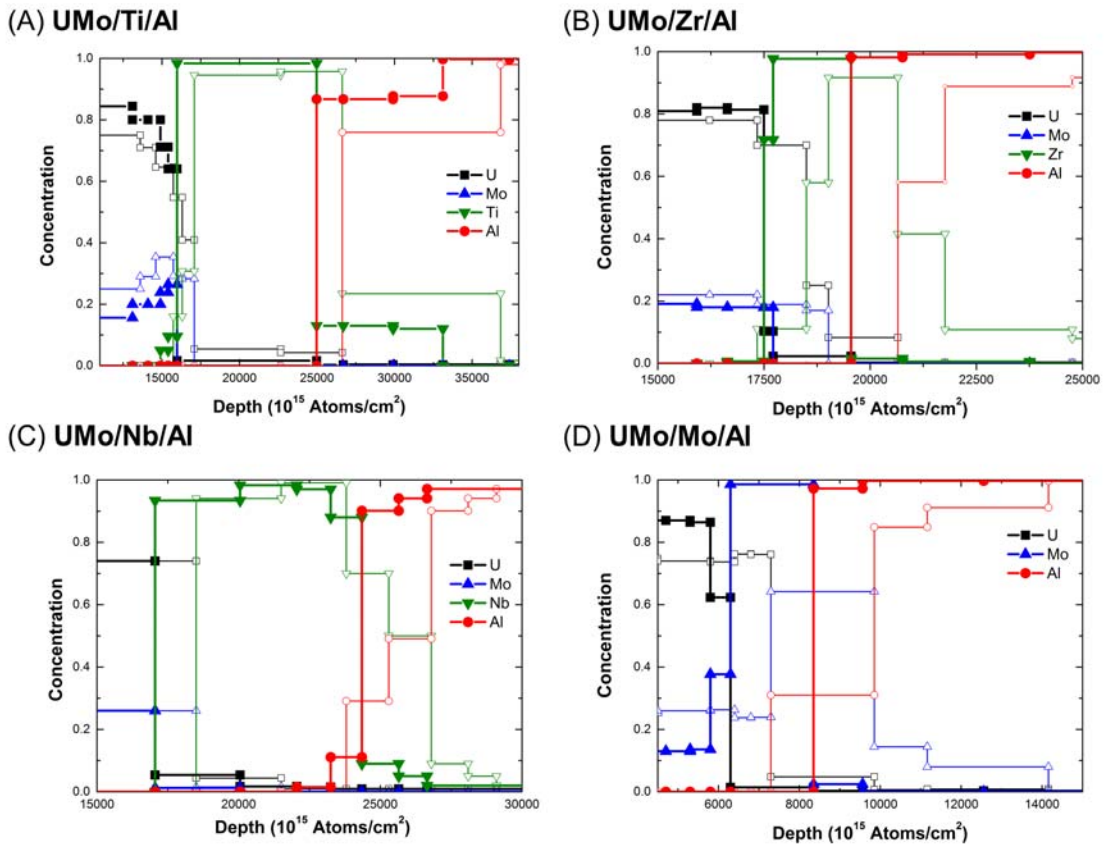

Figure 4: The elemental depth profiles have been derived from RBS spectra by the SIMNRA software [23] at the respective non-irradiated area (solid symbols) and irradiated area (hollow symbols) of UMo/X/Al trilayer samples: X = Ti (A), Zr (B), Nb (C), and Mo (D). In order to observe the intermixing at the interfaces, the elemental depth profiles have been plotted between the UMo/X and the X/Al interfaces. These elemental depth profiles indicate a strong atomic mixing at the interfaces induced by swift heavy ion irradiation.

(A) **UMo region**

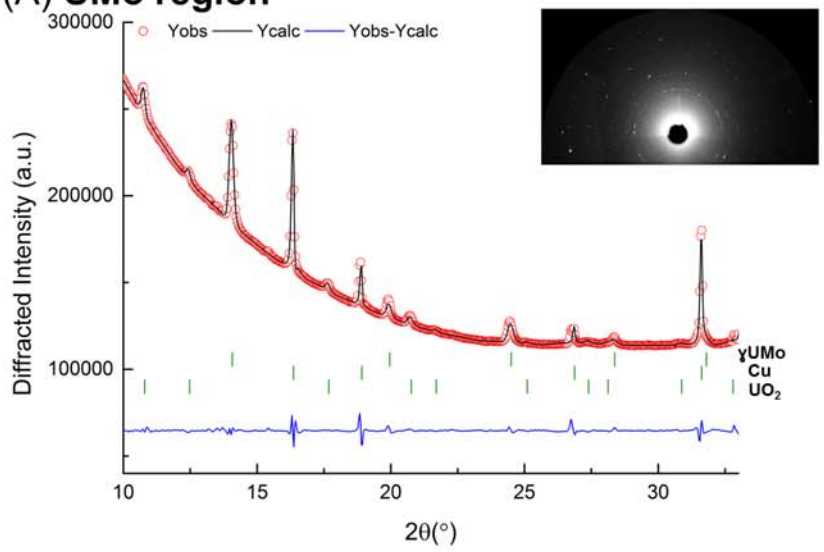

(B) **near UMo/Ti interface**

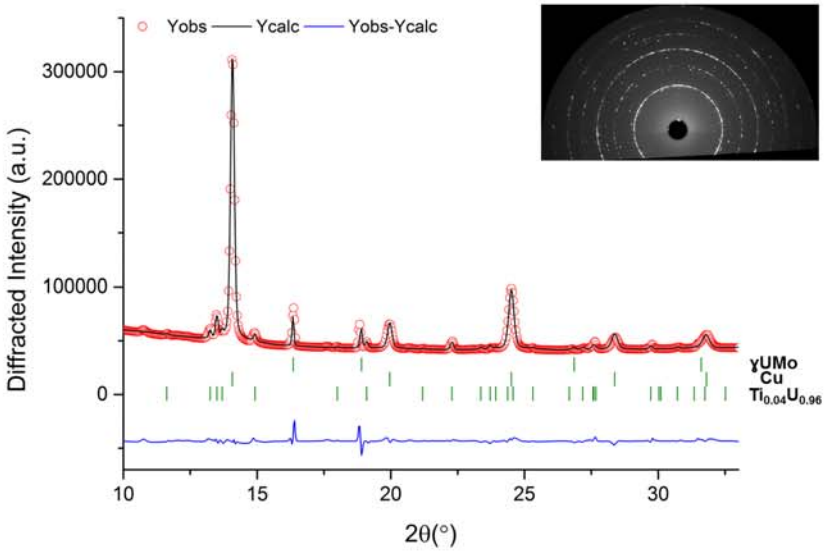

(C) **Ti/Al interface**

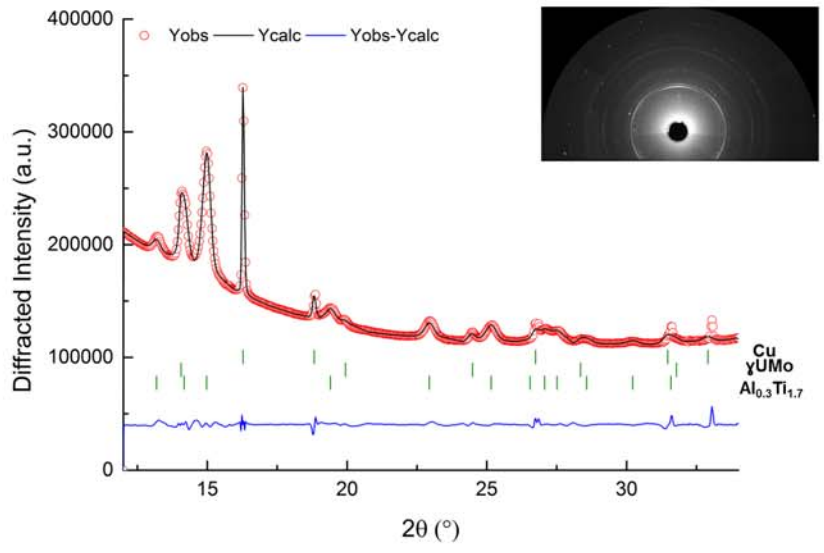

Figure 5: Spatially-resolved μ-XRD patterns of the UMo/Ti/Al trilayer. Observed (open circles) and calculated (solid line) intensities from the UMo region (A); at the UMo/Ti interface (B); at the Ti/Al interface (C) of the UMo/Ti/Al sample. A flat difference profile at the bottom demonstrates a highly reliable agreement of observed intensities with those from Rietveld calculations with all identified phases given within each graphic. The bars indicate their reflection positions including those from the Cu sample holder.

(A) **UMo region**

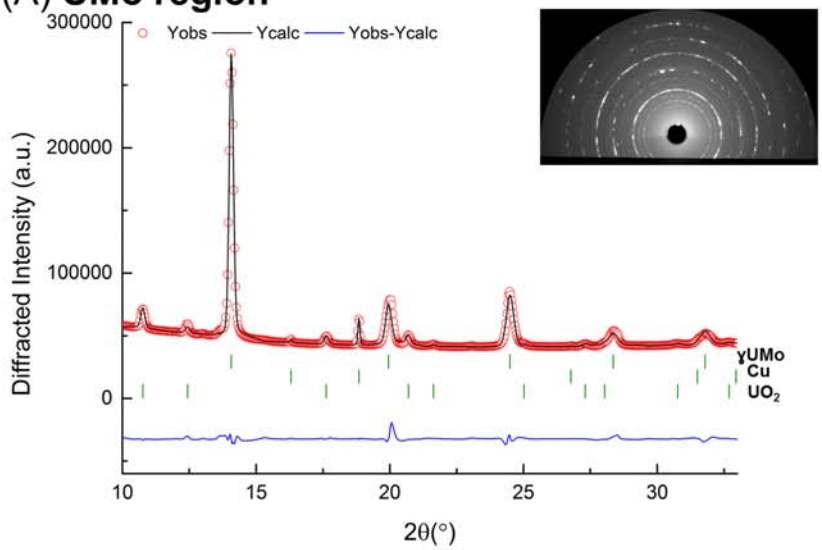

(B) **near UMo/Zr interface**

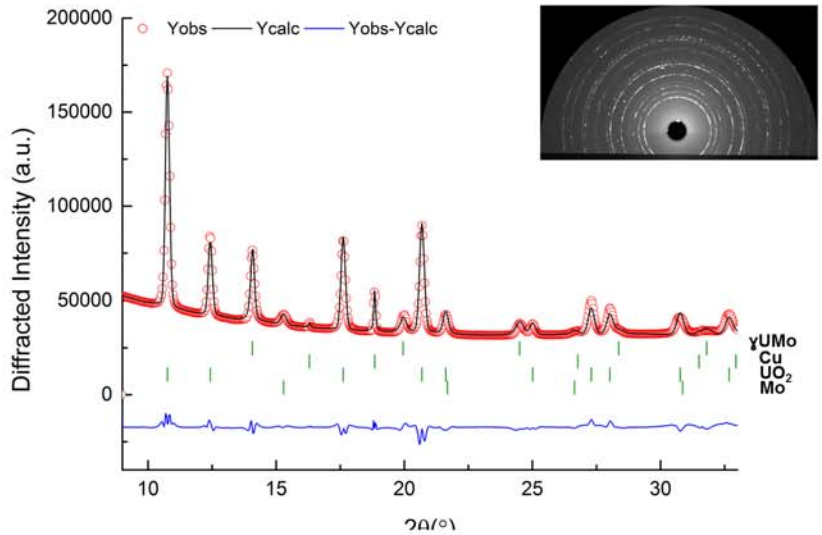

(C) **Zr/Al interface**

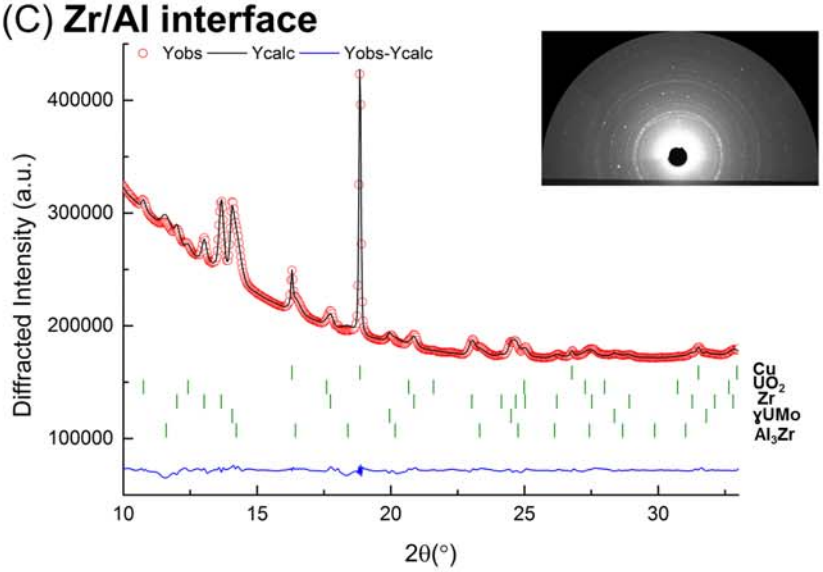

Figure 6: Spatially-resolved μ-XRD patterns of the UMo/Zr/Al trilayer Observed (open circles) and calculated (solid line) μ-XRD patterns from different locations within the UMo/Zr/Al trilayer sample: (A) UMo region; (B) UMo/Zr interfacial region; (C) Zr/Al interfacial region.

(A) **UMo region**

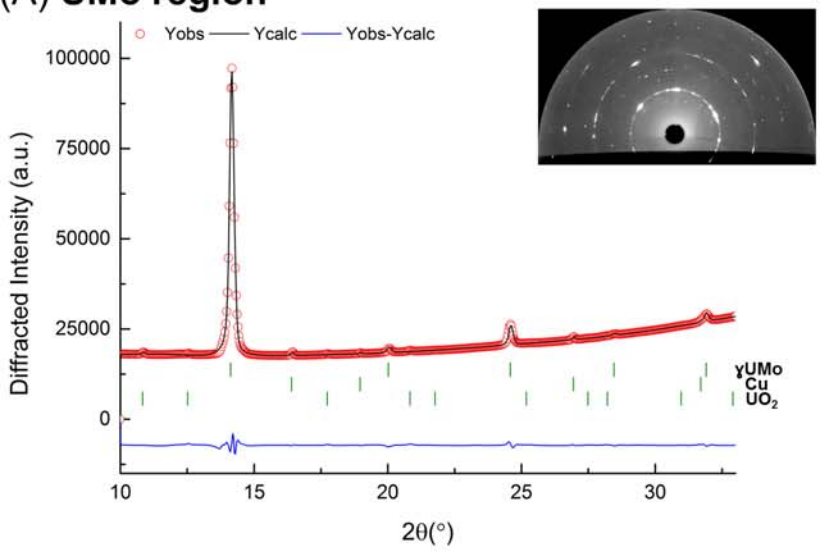

(B) **Nb region**

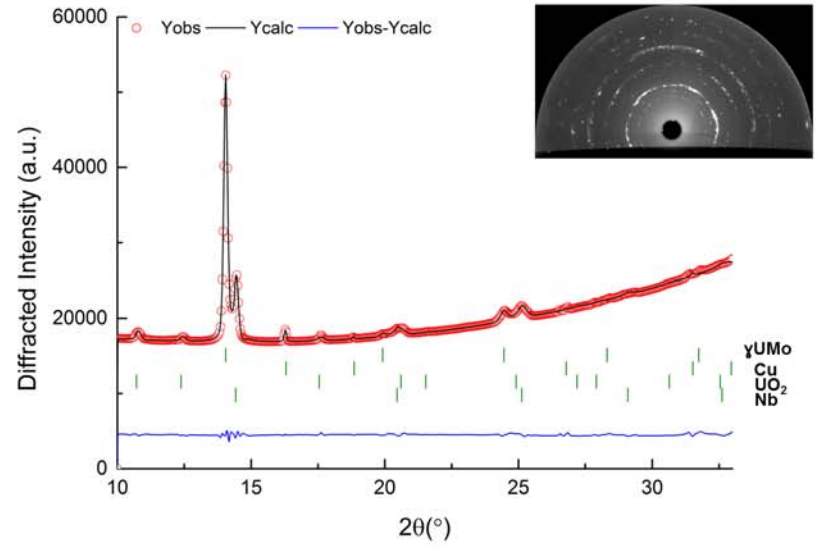

(C) **Nb/Al interface**

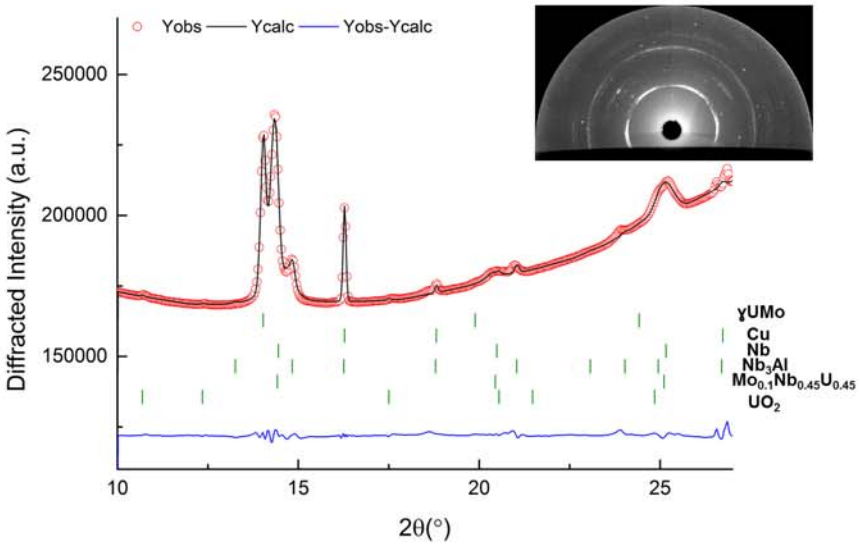

Figure 7: Spatially-resolved μ-XRD patterns of the UMo/Nb/Al trilayer Observed Observed (open circles) and calculated (solid line) μ-XRD patterns from different locations within of the UMo/Nb/Al trilayer sample: (A) UMo region; (B) UMo/Nb interfacial region; (C) Nb/Al interfacial region.

(A) **UMo region**

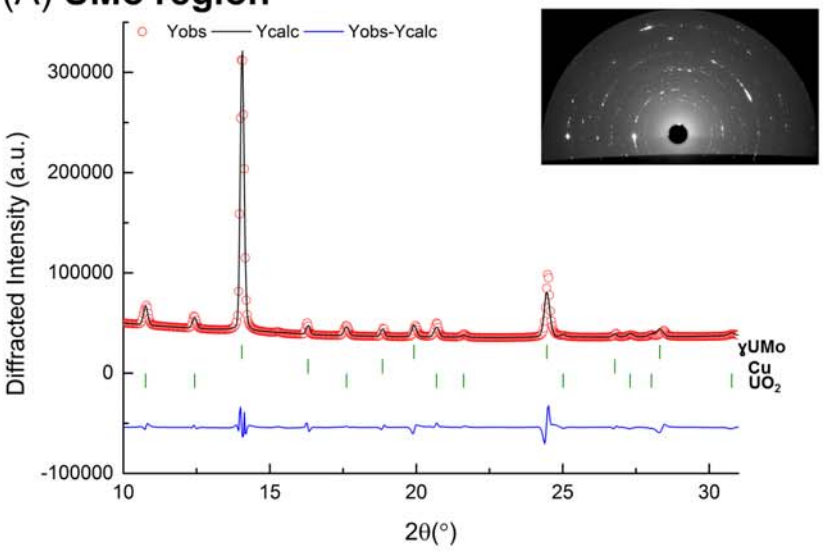

(B) **Mo region**

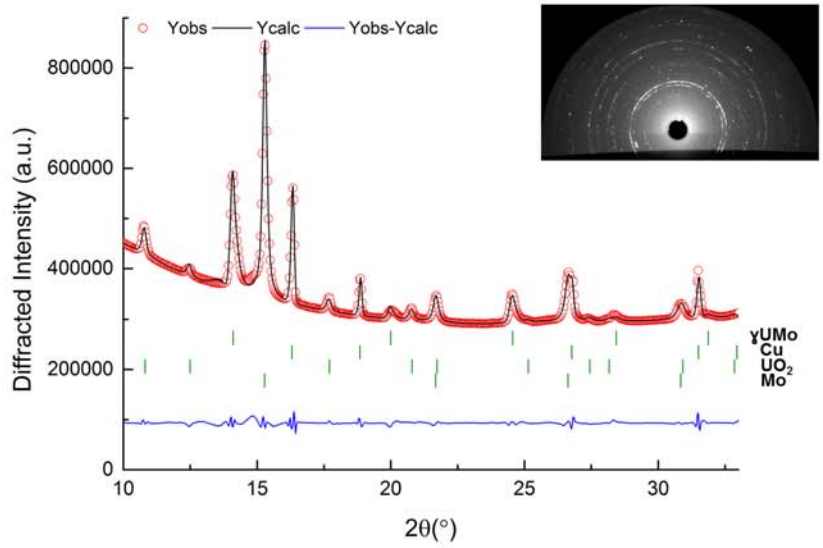

(C) **Mo/Al interface**

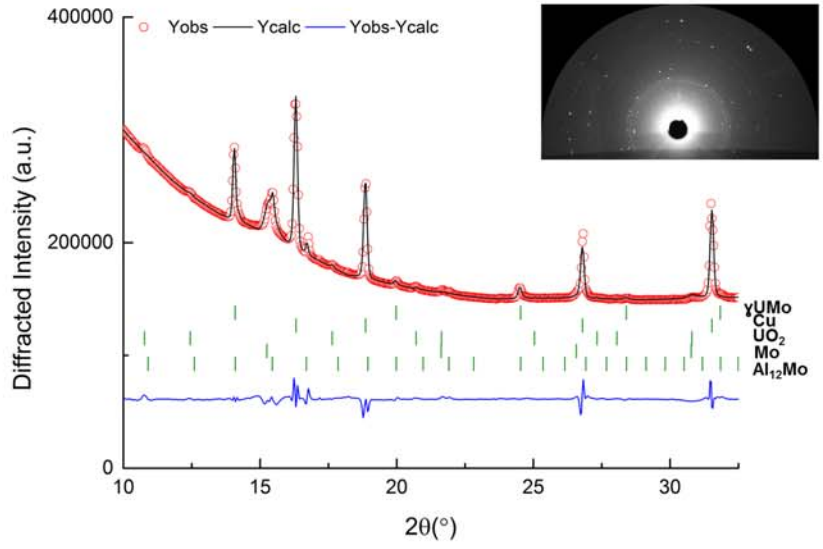

Figure 8: Spatially-resolved μ-XRD patterns of the UMo/Mo/Al trilayer Observed (open circles) and calculated (solid line) μ-XRD patterns from different locations within the UMo/Mo/Al trilayer: (A) UMo region; (B) UMo/Mo interfacial region; (C) Mo/Al interfacial region.

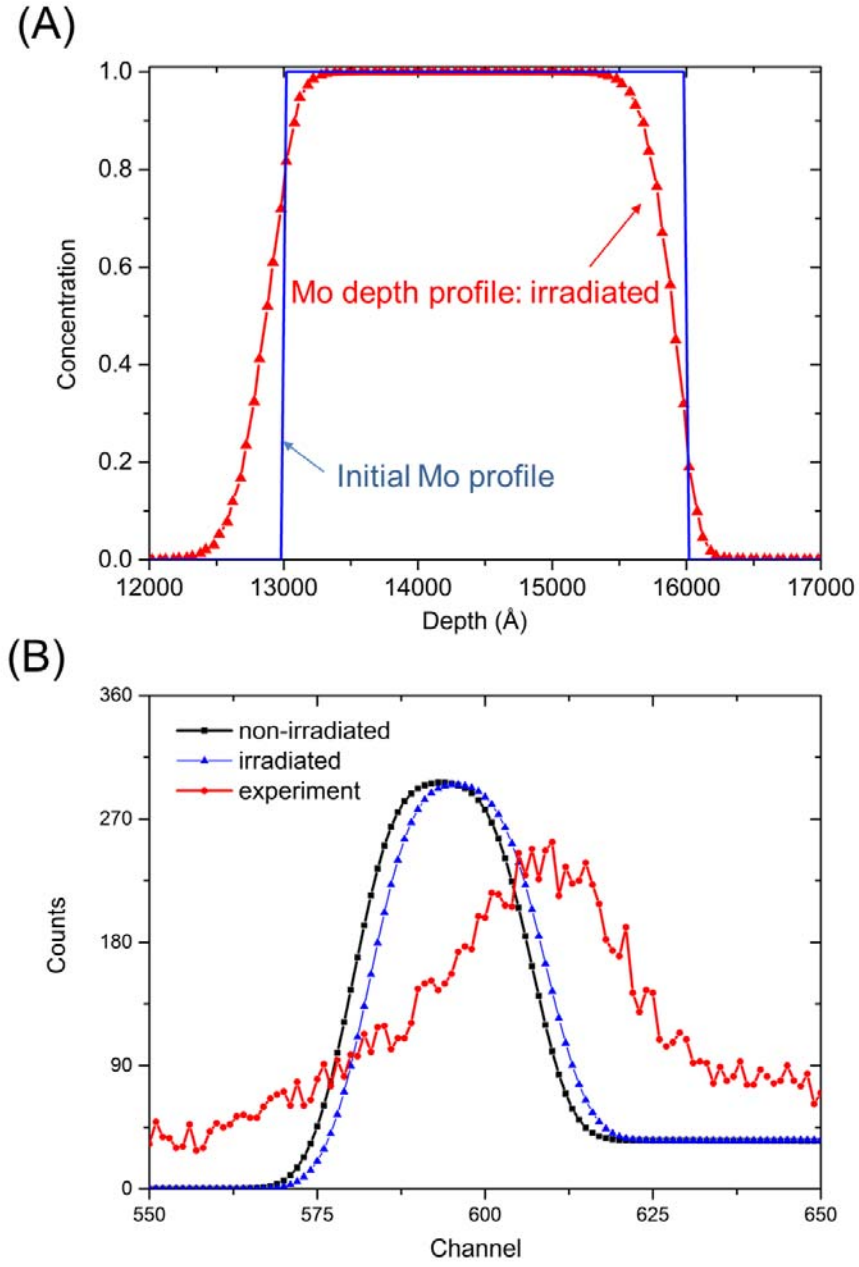

Figure 9: (A) Mo depth profile of the UMo/Mo/Al trilayer evaluated from simulated swift heavy ions irradiation-induced ballistic effects using TRIDYN; (B) A comparison of the TRUDIYN simulation with the observed RBS spectrum of the UMo/Mo/Al trilayer.

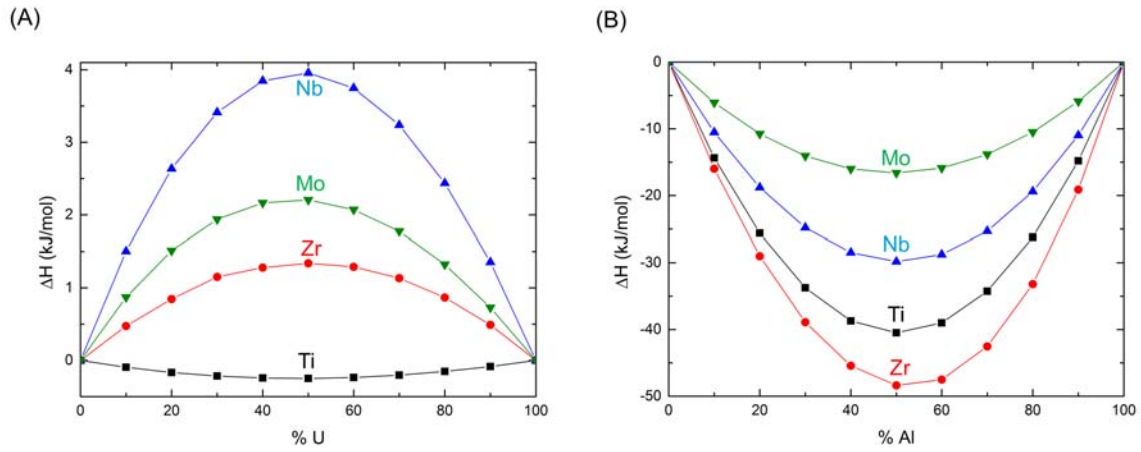

Figure 10: Calculated formation enthalpies of the binary solid solutions U-X (A) and X-Al (B), based on Miedema model [51, 52]. As shown in (A), Ti has a tendency to form a U-Ti alloy whereas other transition metals are relatively inert; Nb has a larger $+\Delta H_m$ against forming the U-Nb alloy in comparison to Zr. On the other hand, the used transition metals are all in favor of forming X-Al solid solutions, in particular Zr, as indicated in the graph (B).